Available online at www.sciencedirect.com
ScienceDirect
Ceramics International 35 (2009) 2679–2685
CERAMICS INTERNATIONAL
www.elsevier.com/locate/ceramint

Effect of sintering temperature on varistor properties and aging characteristics of $ZnO–V_2O_5–MnO_2$ ceramics

Choon-W. Nahm *

Semiconductor Ceramics Lab., Department of Electrical Engineering, Dongeui University, Busan 614-714, Republic of Korea

Received 11 December 2008; received in revised form 30 January 2009; accepted 1 March 2009
Available online 27 March 2009

Abstract

The microstructure, electrical properties, dielectric characteristics, and DC accelerated aging behavior of the ZVM-based varistors were investigated for different sintering temperatures of 800–950 °C. The microstructure of the ZVM-based ceramics consisted of mainly ZnO grain and secondary phase $Zn_3(VO_4)_2$, which acts as liquid-phase sintering aid. The $Zn_3(VO_4)_2$ has a significant effect on the sintered density, in the light of an experimental fact, which the decreases of the $Zn_3(VO_4)_2$ distribution with increasing sintering temperature resulted in the low sintered density. The breakdown field exhibited the highest value (17,640 V/cm) at 800 °C in the sintering temperature and the lowest value (992 V/cm) at 900 °C in the sintering temperature. The nonlinear coefficient exhibited the highest value, reaching 38 at 800 °C and the lowest value, reaching 17 at 850 °C. The varistor sintered at 900 °C exhibited not only high nonlinearity with 27.2 in nonlinear coefficient, but also the highest stability, in which $\%\Delta E_{1\ mA} = -0.6\%$, $\%\Delta\alpha = -26.1\%$, and $\%\Delta \tan\delta = +21.8\%$ for DC accelerated aging stress of 0.85 $E_{1\ mA}$/85 °C/24 h.

Keywords: C. Electrical properties; Microstructure; Ternary system $ZnO–V_2O_5–MnO_2$; Varistor ceramics

1. Introduction

Zinc oxide (ZnO) is a versatile material that possesses wide range of applications for gas sensor, optical devices, grain boundary effect devices, etc. Pure ZnO ceramics exhibits Ohmic properties with the linearity for voltage–current relation when it is sintered without adding impurity intentionally. ZnO varistors exhibit the nonlinear electrical behavior for ceramics formed by sintering ZnO powder with minor additives, such as Bi_2O_3, Pr_6O_{11}, CoO, etc. Microstructurally, the sintering process gives rise to a structure, which consist of semiconducting n-type ZnO grains surrounded by very thin insulating intergranular layers. ZnO varistors possess microstructure of three-dimensional series-parallel network, which a unit structure of ZnO grain (semiconductor)–intergranular layer (insulator)–ZnO grain (semiconductor) distributes to a specified volume size. A unit structure can be equated to a back-to-back zener diode. Unlike a potentiometer, which is manually adjusted, the resistance of a varistor varies automatically in response to change in voltage appearing across it. They are always subjected to a voltage below their breakdown voltage and pass a leakage current. When they are subjected to a voltage above their breakdown voltage, they act as a conductor, discharging surges to ground. When the voltage returns to normal state, they again return to its highly resistive state. As a result, ZnO varistors are devices switching from their highly insulating state to highly conducting state. This nonlinear behavior is due to the presence of a double Schottky barrier formed at the grain boundaries containing many trap states. Owing to the high nonlinearity, the varistors are widely used in the field of overvoltage protection systems from electronic circuits to electric power systems [1,2].

ZnO varistors cannot exhibit a nonlinear behavior without adding the heavy elements with large ionic radii such as Bi, Pr, Ba, etc. Commercial $ZnO–Bi_2O_3$ and $ZnO–Pr_6O_{11}$ systems cannot be co-fired with a Ag inner-electrode (m.p. 961 °C) in multilayered chip components because of the relatively high sintering temperature above 1000 °C [3,4]. Therefore, new varistor ceramics are required in order to use a Ag inner-electrode. Among the various ceramics, one candidate is $ZnO–V_2O_5$ system [5–13]. This system can be sintered at relatively low temperature below 950 °C. This is important for multilayer

* Tel.: +82 51 890 1669; fax: +82 51 890 1664.
E-mail address: cwnahm@dongeui.ac.kr.

0272-8842/$36.00
doi:10.1016/j.ceramint.2009.03.011

chip component applications, because it can be co-sintered with a Ag inner-electrode without using expensive Pd or Pt metals. Therefore, to develop nonlinear ceramics in terms of high performance and manufacturing cost, it is very important to comprehend the influences of additives or sintering processes on nonlinear properties and its stability against various stresses. MnO_2 is often added to $ZnO–Bi_2O_3$ system to improve the varistor properties [14,15]. Also, MnO_2 was found to restrict the abnormal grain growth of ZnO and exhibit better varistor properties in $ZnO–V_2O_5$ system [10,12,13].

In this report, the effect of sintering temperature on the microstructure, electric properties, dielectric characteristics, and DC accelerated aging behavior of the $ZnO–V_2O_5–MnO_2$ (ZVM)-based varistors was examined and some remarkable results were obtained.

2. Experimental procedure

2.1. Sample preparation

Reagent-grade raw materials were used for preparing the samples with ternary composition expression, such as 97.5 mol% ZnO + 0.5 mol% V_2O_5 + 2.0 mol% MnO_2. Raw materials were mixed by ball milling with zirconia balls and acetone in a polypropylene bottle for 24 h. The mixture was dried at 120 °C for 12 h. The mixture was stirred together with acetone and polyvinyl butyl alcohol (PVB) binder into beaker. After drying, the powder was granulated by sieving 100-mesh screen to produce starting powder. The powder was uniaxially pressed into discs of 10 mm in diameter and 1.5 mm in thickness at a pressure of 80 MPa. The discs were covered with raw powder in alumina crucible, sintered at four fixed sintering temperatures (800, 850, 900, and 950 °C) in air for 3 h, and furnace-cooled to room temperature. The sintered samples were lapped and polished to 1.0 mm thickness. The size of the final samples was about 8 mm in diameter and 1.0 mm in thickness. Both faces of the samples were coated in a silver paste and the ohmic contact of electrodes was formed by heating at 600 °C for 10 min. The size of electrodes was 5 mm in diameter.

2.2. Microstructure measurement

Both sides of the samples were lapped and ground with SiC paper and polished with 0.3 μm-Al_2O_3 powder to a mirror-like surface. The polished samples were chemically etched into $1HClO_4$:$1000H_2O$ for 25 s at 25 °C. The surface microstructure was examined by a scanning electron microscope (SEM, Hitachi S2400, Japan). The average grain size (d) was determined by the lineal intercept method such as the expression, $d = 1.56L/MN$ [16], where L is the random line length on the micrograph, M is the magnification of the micrograph, and N is the number of the grain boundaries intercepted by lines. The crystalline phases were identified by powder X-ray diffraction (XRD, Model D/max 2100, Rigaku, Japan) with CuK_α radiation. The sintered density (ρ) was measured by the Archimedes method.

2.3. Electrical measurement

The electric field–current density (E–J) characteristics were measured using an I–V source/measure unit (Keithley 237). The

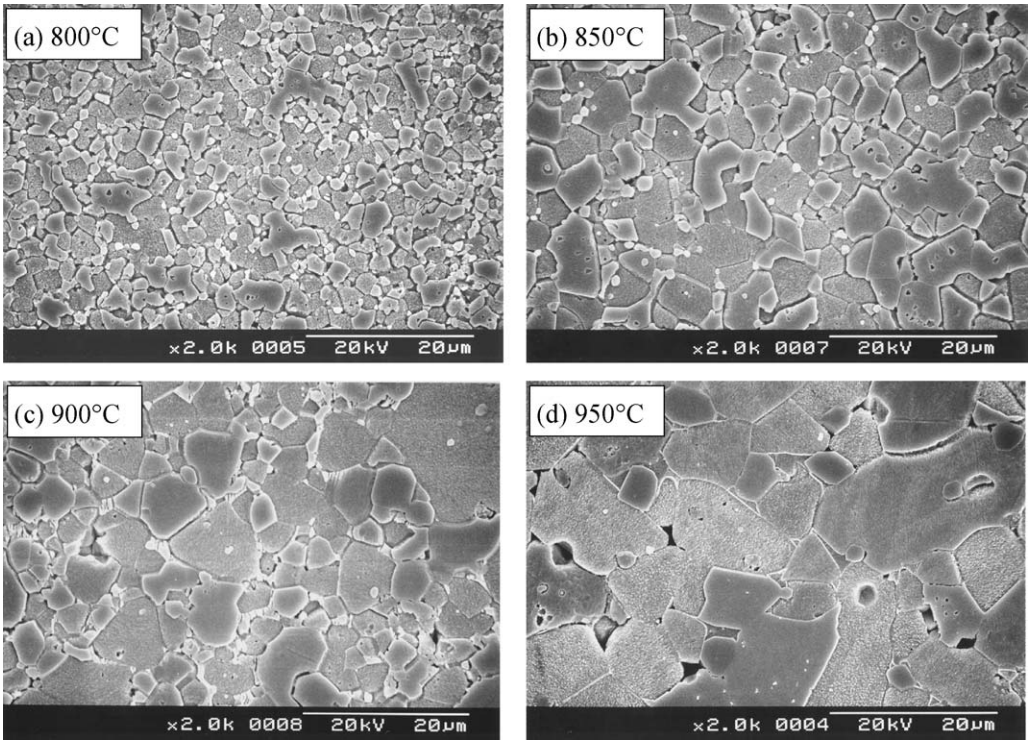

Fig. 1. SEM micrographs of the ZVM-based ceramics for different sintering temperatures.

breakdown field ($E_{1\ mA}$) was measured at 1.0 mA/cm^2 and the leakage current density (J_L) was measured at 0.8 $E_{1\ mA}$. In addition, the nonlinear coefficient (α) is defined by the empirical law, $J = KE^{\alpha}$, where J is the current density, E is the applied electric field, and K is a constant. α was determined in the current density range 1.0–10 mA/cm^2, where $\alpha = 1/(\log E_2 - \log E_1)$, and E_1 and E_2 are the electric fields corresponding to 1.0 and 10 mA/cm^2, respectively.

2.4. Dielectric measurement

The dielectric characteristics, such as the apparent dielectric constant (ε'_{APP}) and dissipation factor (tan δ) were measured in the range of 100 Hz to 2 MHz using a RLC meter (QuadTech 7600).

2.5. DC accelerated aging measurement

The DC accelerated aging test was performed for stress state of 0.85 $E_{1\ mA}$/85 °C/24 h. Simultaneously, the leakage current was monitored at intervals of 1 min during stressing using an *I–V* source/measure unit (Keithley 237). The degradation rate coefficient (K_T) was calculated from the expression $I_L = I_{Lo} + K_T t^{1/2}$ [17], where I_L is the leakage current at stress time (t) and I_{Lo} is I_L at $t = 0$. Five samples (sintered at the same sintering temperature) were used for all electrical measurements and their average value is presented.

3. Results and discussion

Fig. 1 shows the SEM micrographs of the ZVM-based ceramics for different sintering temperatures. The surface morphology was clearer than the morphology reported and revealed a clear grain shape [8,10]. It can be seen that the grain size remarkably increases with the increase of sintering temperature. The average grain size increased from 2.1 to 10.1 μm. ZnO grains could probably grow rapidly in the presence of a V_2O_5-rich liquid phase because the melting point of V_2O_5 is 690 °C [5]. Sintered density slightly increased up to 850 °C, whereas the further increases decreased to 5.44 g/cm^3 (theoretical density 5.78 g/cm^3 for ZnO) at 950 °C. It is presumed that the decrease of sintered density is attributed to the volatility of V-species for V_2O_5 with low melting point. The XRD patterns of the ZVM-based ceramics for different sintering temperatures are shown in Fig. 2. These patterns revealed the presence of $Zn_3(VO_4)_2$ as a secondary phase (small white part in Fig. 1), in addition to the main hexagonal ZnO [7–10]. The revealed phases are identical to those in the binary ZnO–V_2O_5 system. The $Zn_3(VO_4)_2$ is formed by liquid-phase sintering agent, V_2O_5 and acts as liquid-phase sintering aid [5,6]. It is suggested that the liquid phase of $Zn_3(VO_4)_2$ enhances densification of ZnO matrix. It should be noted that the peak of secondary phase $Zn_3(VO_4)_2$ gradually decreased with the increase of sintering temperature. This is attributed to the decrease of $Zn_3(VO_4)_2$ distribution due to the volatility of V_2O_5. On the other hand, no secondary phase related to MnO_2 was detected. No peak for the V-species is found in the grain

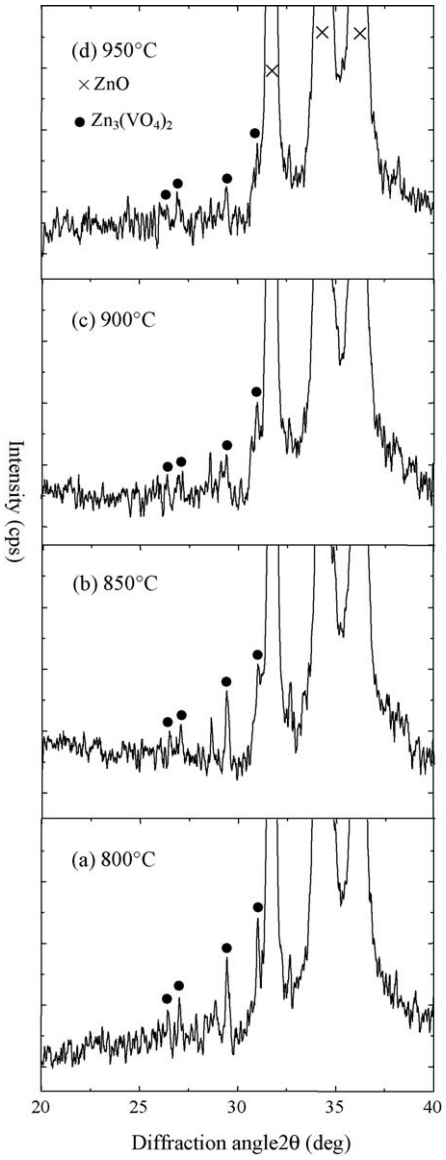

Fig. 2. XRD patterns of the ZVM-based ceramics.

interior within EDX detection limit, though the ion radius of V is smaller than that of Zn. This means the V-species is not dissolved into the ZnO grain. However, the Mn-species was found to exist at the grain interior, in addition to Zn. On the other hand, it is found that the grain boundaries contain V- and Mn-species. As a result, the Mn-species exist in both grain and grain boundaries. The detailed microstructural parameters are summarized in Table 1.

Fig. 3 shows the electric field–current density (*E–J*) characteristics of the ZVM-based varistors for different sintering temperatures. The varistor properties are characterized by non-ohmicity in the *E–J* characteristics. The curves that show the conduction characteristics are divided into two regions: a linear region before breakdown field and a nonlinear region after breakdown field. Conduction in linear region is dominated by thermionic emission over a Schottky barrier at grain boundaries and conduction in breakdown region is dominated by Folower–Nordheim field emission through a

Table 1
Microstructure, electrical and dielectric characteristic parameters of the ZVM-based varistors for different sintering temperatures.

Sintering temperature (°C)	d (μm)	ρ (g/cm^3)	$E_{1\ mA}$ (V/cm)	$_{gb}$ (V/gb)	α	J_L (mA/cm^2)	ε'_{APP} (1 kHz)	tan δ (1 kHz)
800	2.1	5.56	17,640	3.7	38.1	0.14	135.2	0.0781
850	4.4	5.59	7,881	3.5	17.0	0.27	299.8	0.1838
900	5.2	5.51	992	0.5	27.2	0.17	1163.5	0.3160
950	10.1	5.44	2,430	2.5	32	0.11	800.9	0.2090

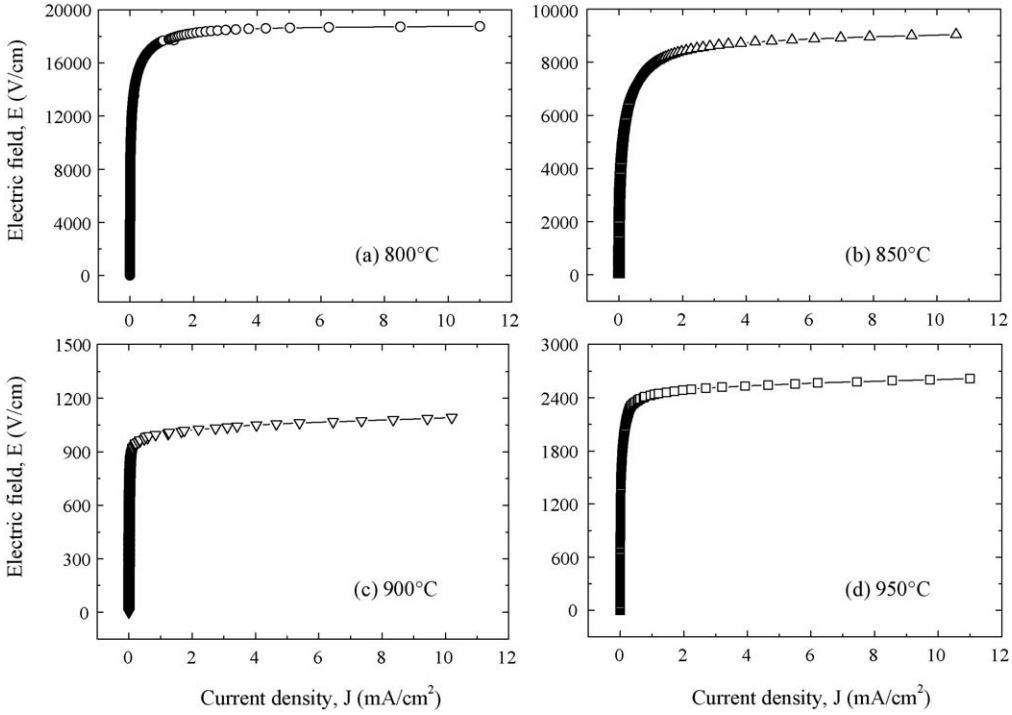

Fig. 3. *E–J* characteristics of the ZVM-based varistors for different sintering temperatures.

Schottky barrier. The sharper the knee of the curves between the two regions, the better the nonlinear properties. The varistors sintered at 800, 900, and 950 °C exhibited nearly similar shape of characteristic curves and show high nonlinearity. However, it can be forecasted that the varistor sintered at 850 °C exhibit low nonlinear properties by showing more round-like knee, compared with others. Therefore, the sintering temperature seems to affect the varistor properties.

The breakdown field ($E_{1\ mA}$) remarkably decreased from 17,640 to 992 V/cm up to 900 °C with the increase of sintering temperature, whereas the further increase caused the increase of $E_{1\ mA}$, reaching 2430 V/cm at 950 °C. As the sintering temperature increased, the decrease of $E_{1\ mA}$ is attributed to the decrease in the number of grain boundaries caused by the increase in the ZnO grain size because the varistor is a device, which depends on thickness of the sample. On the contrary, as the sintering temperature increased in the range of 900–950 °C, the increase of $E_{1\ mA}$ is attributed to the abrupt increase of breakdown voltage per grain boundary (v_{gb}). The v_{gb} is calculated by the following equation: $V_{1\ mA} = N_{gb} \cdot v_{gb} = (D/d)v_{gh}$, where $V_{1\ mA}$ is breakdown voltage, N_b is the number of grain boundaries, d is the average grain size, and D is the thickness of sample. The v_{gb} of varistors sintered at 800, 900, and 950 °C was in the range of 2.5–3.7 V, whereas the v_{gb} was only 0.5 V for varistor sintered at 900 °C.

The nonlinear coefficient (α) values are derived from the *E–J* curves. The α value of the ZVM-based varistors remarkably decreased from 38.1 to 17 with the increase of sintering temperature up to 850 °C. The further increases caused the increase of α, reaching 32 at 950 °C. It can be seen that the sintering temperature has a significant effect on the nonlinear properties in the light of the α variation. On the other hand, the current density (J_L) increased from 0.14 to 0.27 mA/cm^2 with the increase of sintering temperature up to 850 °C. The further increases caused the decrease of J_L, reaching 0.11 mA/cm^2 at 950 °C. This is attributed to the increase of α, which is directly related to the Schottky barrier at grain boundaries. The J_L variation with sintering temperature was opposite to the tendency of α variation. The detailed *E–J* characteristic parameters are summarized in Table 1.

Fig. 4 shows the apparent dielectric constant (ε'_{APP}) and dissipation factor (tan δ) of the ZVM-based varistors for different sintering temperatures. With increasing frequency for all varistors, the ε'_{APP} decreased with less sharp dispersive drop which is closely associated with the polarization of dielectrics. On the whole, the decreasing rate of the ε'_{APP} exhibited to

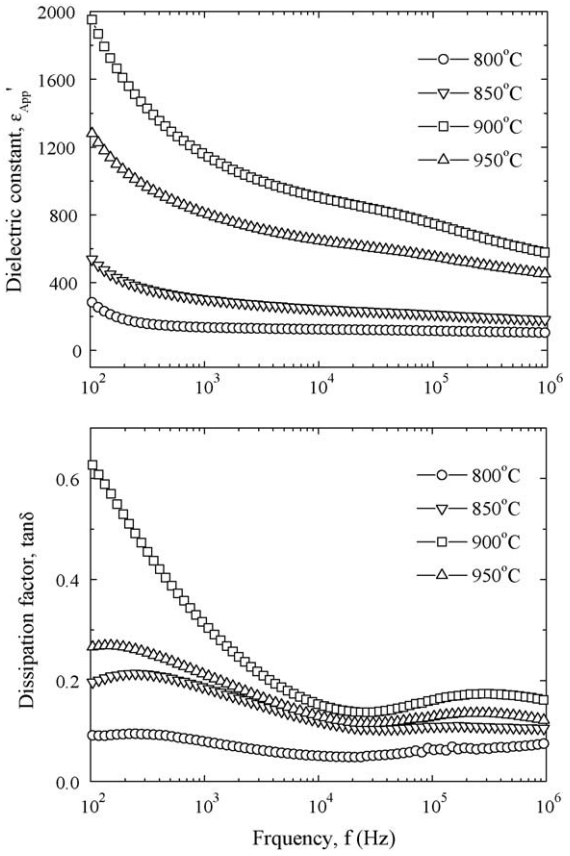

Fig. 4. Dielectric characteristics of the ZVM-based varistors for different sintering temperatures.

increase with the increase of sintering temperature. It is assumed that this is attributed to the decrease of the number of dipole, which can follow to test frequency. The ε'_{APP} increased in the range of overall frequency up to 900 °C with the increase of sintering temperature. The further increases caused the decrease of ε'_{APP}. This is directly related to the average grain size and depletion layer width, as can be seen in the following equation, $\varepsilon'_{APP} = \varepsilon_g(d/t)$, where ε_g is the dielectric constant of ZnO (8.5), d is the average grain size, and t is the depletion layer width of the both sides at the grain boundaries. Dielectric constant can expect to increase because the d increases with increasing sintering temperature. However, the dielectric constant of the varistor sintered at 900 °C is greater than that of the varistor sintered at 950 °C. It is assumed that this is attributed to the depletion layer width because ε'_{APP} is related to d/t ratio in $\varepsilon'_{APP} = \varepsilon_g(d/t)$. That is, it is presumed that the d/t at 900 °C is larger than that of 950 °C, based on experimental data. The ε'_{APP} at 1 kHz increased from 135.2 to 1163.5 at 900 °C, whereas it decreased to 800.9 at 950 °C. On the other hand, the tan δ decreased until the vicinity of 20 kHz with increasing frequency, which exhibits dielectric dispersion peak in the vicinity of 300 kHz, and thereafter again decreased. The tan δ at 1 kHz value increased from 0.0781 to 0.3160 at 900 °C, whereas it decreased to 0.2090 at 950 °C. The detailed dielectric characteristic parameters are summarized in Table 1.

In practical varistor applications, two important factors that need to be considered are the nonlinearity of V–I properties and its stability. The varistors begin to degrade because of gradually increasing leakage current with stress time. Eventually, they result in thermal runaway and the loss of varistor function. Therefore, the electrical stability of the varistor is more important than any other properties. In this viewpoint, in addition to nonlinearity, the electrical stability is technologically a very important characteristic of ZnO varistors [4].

Fig. 5 shows leakage current (I_L) behavior of the ZVM-based varistors during DC accelerated aging stress of 0.85 $E_{1\ mA}$/85 °C/24 h. The I_L gradually increased with increasing stress time and this shows that the varistors are gradually degraded. The varistors sintered at 800 and 850 °C resulted in the thermal runaway within short time. These exhibited to be very weak against DC accelerated aging stress. In general, the low sintered density and high leakage current greatly decrease the resistance for the stability. The former decreases the number of conduction path and eventually leads to the concentration of current. The latter leads to repetition cycle between joule heating and leakage current. In the light of above state, the varistors sintered at 800 and 850 °C were expected to exhibit the high stability. However, contrary to expectation, it exhibited a very low stability. If so, why these samples exhibit thermal runaway though it is high sintered density and low leakage current? Presumably, this seems to be related to secondary phase $Zn_3(VO_4)_2$. The increase of $Zn_3(VO_4)_2$ distribution decreases the cross-sectional area of conduction path at grain boundary and eventually leads to the concentration of current. As a result, it is assumed that $Zn_3(VO_4)_2$ of secondary phase affects stability against stress. It is difficult to apply as a varistor because a bad stability even if the nonlinear properties are good, in particular, for the varistor with a high nonlinearity, sintered at 800 °C. On the contrary, the varistors sintered at 900 and 950 °C were found to exhibit a good stability without thermal runaway during specified stress time period. The stability of the samples can be estimated by the degradation rate coefficient (K_T), indicating the degree of aging. This exhibits the slope of leakage current for the stress time. The lower the K_T leads to the higher the stability. The K_T values of the varistors sintered at 900 and 950 °C exhibited 3.8

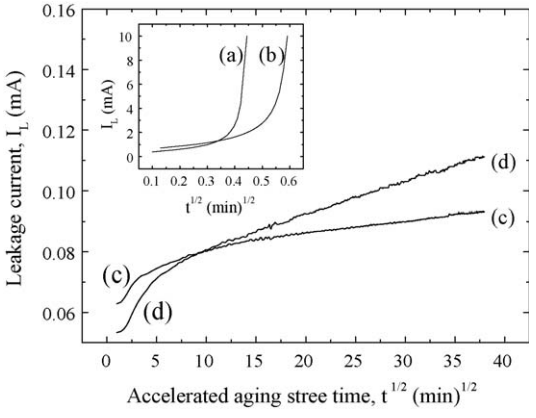

Fig. 5. Leakage current behavior during DC accelerated aging stress of the ZVM-based varistors for different sintering temperatures.

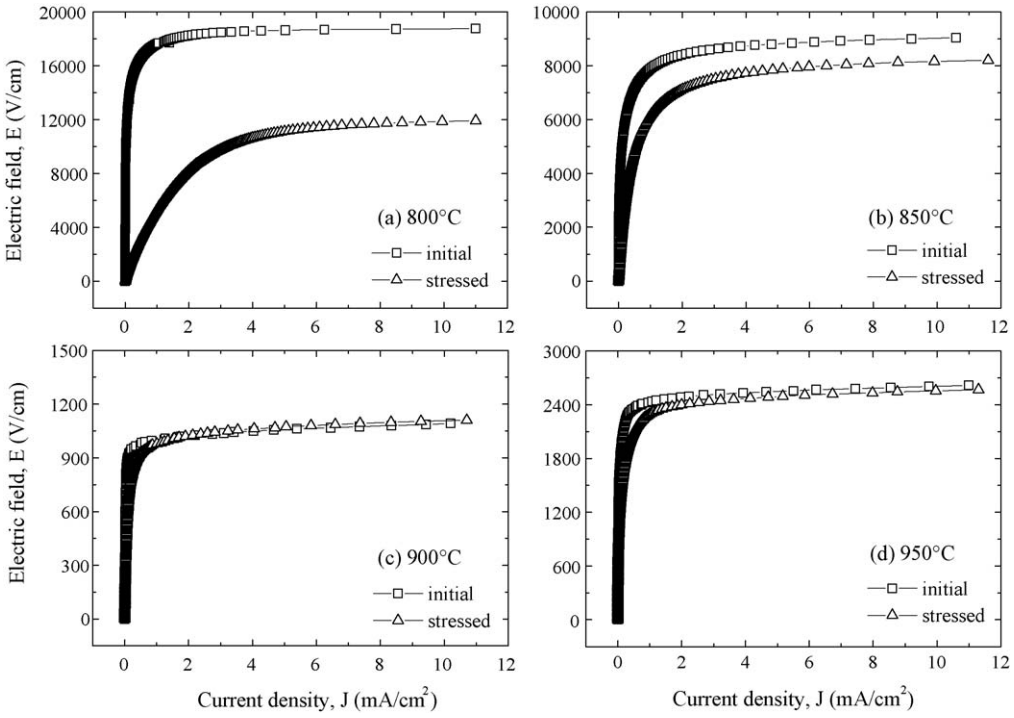

Fig. 6. *E–J* characteristic behavior before and after DC accelerated aging stress of the ZVM-based varistors for different sintering temperatures.

and 9.0 μA $h^{-1/2}$, respectively. As a result, the varistors sintered at 900 °C seems to exhibit high stability than the varistors sintered at 950 °C. In the light of the facts, it can be seen that the resistance against DC accelerated aging stress is greatly affected by the sintering temperature.

Fig. 6 shows *E–J* characteristic behavior before and after DC accelerated aging stress of the ZVM-based varistors for different sintering temperatures. It can be seen that the variation of *E–J* curves after stress is strongly affected by sintering temperature. The varistor sintered at 900 °C exhibited very small variation in *E–J* curves after stress and the degree of variation coincided with the variation of K_T value with the sintering temperature. The $E_{1\ mA}$ and α values before and after stress as a function of sintering temperature is shown in Figs. 7 and 8, respectively. The decreasing rate of $E_{1\ mA}$ after stress decreased in the order of 800, 850, 950, and 900 °C. In particular, the varistor sintered at 900 °C exhibited the lowest variation rate of $E_{1\ mA}$, reaching $\Delta E_{1\ mA} = -0.6\%$. After stress, the decreasing rate of α value exhibited nearly similar tendency to that of $E_{1\ mA}$. The varistor sintered at 800 °C exhibited extremely bad nonlinear properties by decreasing to $\alpha = 2.8$ after stress. On the contrary, the varistors sintered at 900 and 950 °C exhibited high nonlinearity by exhibiting $\alpha > 20$ after stress. On the other hand, in dielectric characteristics, the ε'_{APP} is not nearly affected by DC accelerated aging stress, as shown in Fig. 9. This is based on the fact that the grain size and depletion layer width are not changed by DC stress. On the contrary, the tan δ after stress increased compared with that before stress, as shown in Fig. 10. Of the varistors, the varistor 900 °C exhibited the lowest variation rate, with +21.8% in %Δ tan δ.

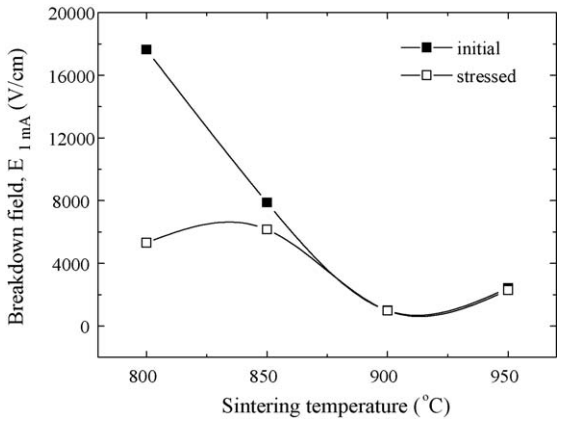

Fig. 7. Breakdown field behavior before and after DC accelerated aging stress of the ZVM-based varistors as a function of sintering temperatures.

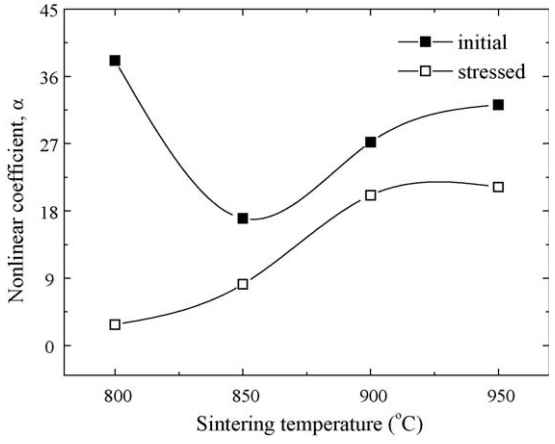

Fig. 8. Nonlinear coefficient behavior before and after DC accelerated aging stress of the ZVM-based varistors as a function of sintering temperatures.

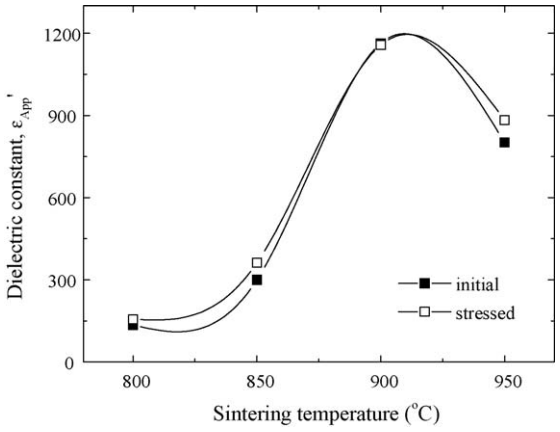

Fig. 9. Dielectric constant behavior before and after DC accelerated aging stress of the ZVM-based varistors as a function of sintering temperatures.

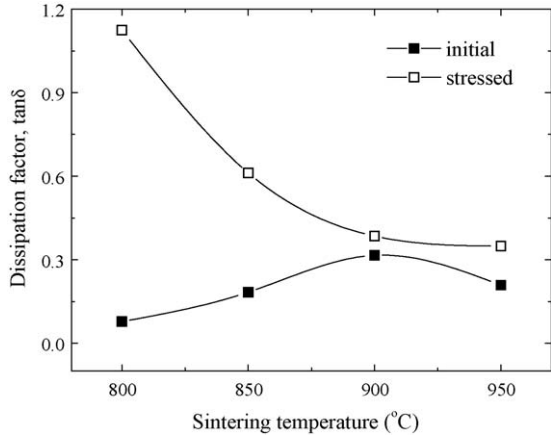

Fig. 10. Dissipation factor behavior before and after DC accelerated aging stress of the ZVM-based varistors as a function of sintering temperatures.

4. Conclusions

The effect of sintering temperature on microstructure, electrical properties, dielectric characteristics, and DC accelerated aging behavior of the ZVM-based varistors was investigated in the range of 800–950 °C. The microstructure of the ZVM-based varistors consisted of ZnO grain as a primary phase and $Zn_3(VO_4)_2$ as a secondary phase, which acts as liquid-phase sintering aid. The $Zn_3(VO_4)_2$ has a significant effect on the sintered density, in the light of an experimental fact, which the decrease of the $Zn_3(VO_4)_2$ distribution with increasing sintering temperature resulted in the low sintered density. The breakdown field exhibited the highest value as 17,640 V/cm at 800 °C and the lowest value of 992 V/cm at 900 °C. The nonlinear coefficient exhibited the highest value, reaching 38 at 800 °C and the lowest value, reaching 17 at 850 °C. The varistor sintered at 900 °C exhibited not only high nonlinearity with 27.2 in nonlinear coefficient, but also the highest stability, in which $\%\Delta E_{1\ mA} = -0.6\%$, $\%\Delta\alpha = -26.1\%$, and $\%\Delta \tan\delta = +21.8\%$ for DC accelerated aging stress of 0.85 $E_{1\ mA}$/85 °C/24 h. Conclusively, it is noted that the ZVM-based varistor is a potential material for multilayer chip varistors with an Ag inner-electrode.

References

[1] L.M. Levinson, H.R. Philipp, Zinc oxide varistor—a review, Am. Ceram. Soc. Bull. 65 (1986) 639–646.
[2] T.K. Gupta, Application of zinc oxide varistor, J. Am. Ceram. Soc. 73 (1990) 1817–1840.
[3] C.-W. Nahm, The nonlinear properties and stability of ZnO–Pr_6O_{11}–CoO–Cr_2O_3–Er_2O_3 ceramic varistors, Mater. Lett. 47 (2001) 182–187.
[4] C.-W. Nahm, Nonlinear properties and stability against DC accelerated aging stress of praseodymium oxide-based ZnO varistors by Er_2O_3 doping, Solid State Commun. 126 (2003) 281–284.
[5] J.-K. Tsai, T.-B. Wu, Non-ohmic characteristics of ZnO–V_2O_5 ceramics, J. Appl. Phys. 76 (1994) 4817–4822.
[6] J.-K. Tsai, T.-B. Wu, Microstructure and nonohmic properties of binary ZnO–V_2O_5 ceramics sintered at 900 °C, Mater. Lett. 26 (1996) 199–203.
[7] C.-S. Chen, C.-T. Kuo, T.-B. Wu, I.-N. Lin, Microstructure and electrical properties of V_2O_5-based multicomponent ZnO varistors prepared by microwave sintering preprocess, Jpn. J. Appl. Phys. 37 (1997) 1169–1175.
[8] C.-T. Kuo, C.-S. Chen, I.-N. Lin, Microstructure and nonlinear properties of microwave-sintered ZnO–V_2O_5 varistors. II. Effect of Mn_3O_4 doping, J. Am. Ceram. Soc. 81 (1998) 2949–2956.
[9] H.-H. Hng, K.M. Knowles, Characterisation of $Zn_3(VO_4)_2$ phases in V_2O_5-doped ZnO varistors, J. Eur. Ceram. Soc. 19 (1999) 721–726.
[10] H.-H. Hng, P.-L. Chan, Effects of MnO_2 doping in V_2O_5-doped ZnO varistor system, Mater. Chem. Phys. 75 (2002) 61–66.
[11] H.-H. Hng, L. Halim, Grain growth in sintered ZnO^{-1} mol% V_2O_5 ceramics, Mater. Lett. 57 (2003) 1411–1416.
[12] C.-W. Nahm, Microstructure and varistor properties of ZnO–V_2O_5–MnO_2-based ceramics, J. Mater. Sci. 42 (2007) 8370–8373.
[13] C.-W. Nahm, Microstructure and electrical properties of vanadium-doped zinc oxide-based non-ohmic resistors, Solid State Commun. 143 (2007) 453–456.
[14] G.S. Pike, S.R. Kurtz, P.L. Gourley, H.R. Philipp, L.M. Levinson, J. Appl. Phys. 57 (1985) 5512–5518.
[15] L.M. Levinson, Advances in varistor technology, Am. Ceram. Soc., (Westerville, OH) 3 (1989) 31–53.
[16] J.C. Wurst, J.A. Nelson, Lineal intercept technique for measuring grain size in two-phase polycrystalline ceramics, J. Am. Ceram. Soc. 55 (1972) 109–111.
[17] J. Fan, R. freer, Deep level transient spectroscopy of zinc oxide varistors doped with aluminum oxide and/or silver oxide, J. Am. Ceram. Soc. 77 (1994) 2663–2668.